JOURNAL OF AGRICULTURAL AND FOOD CHEMISTRY

J. Agric. Food Chem. **2008,** *56,* 5129–5137 **5129**

Effects of Brine Salting with Regard to Raw Material Variation of Atlantic Salmon (*Salmo salar*) Muscle Investigated by Fourier Transform Infrared Microspectroscopy

ULRIKE BÖCKER,*,†,‡ ACHIM KOHLER,†,§,|| IDA G. AURSAND,⊥,# AND RAGNI OFSTAD†

Centre for Biospectroscopy and Data Modelling, Matforsk AS, Norwegian Food Research Institute, Osloveien 1, N-1430 Ås, Norway, Department of Chemistry, Biotechnology and Food Science, Norwegian University of Life Sciences, P.O. Box 5003, N-1432 Ås, Norway, CIGENE, Centre for Integrative Genetics, Norwegian University of Life Sciences, N-1432 Ås, Norway, Department of Mathematical Sciences and Technology (IMT), Norwegian University of Life Sciences, N-1432 Ås, Norway, SINTEF Fisheries and Aquaculture AS, Brattørkaia 17 B, N-7465 Trondheim, Norway, and Department of Biotechnology, Norwegian University of Science and Technology, N-7941 Trondheim, Norway

Atlantic salmon fillets differing with regard to raw material characteristics (prerigor, postrigor, frozen/thawed) and salt content were investigated by FT-IR microspectroscopy and light microscopy. Local variation within each salmon fillet was further taken into account by sampling from the head and tail part separately as they vary in fat and moisture content. The highest salt uptake was achieved for frozen/thawed quality during brine-salting with 16% NaCl for 4 h, while the uptake was least for prerigor fish. At the same time, salting caused muscle fiber swelling of about 10% for both frozen/thawed and postrigor qualities. Differences in the FT-IR amide I spectral region were observed implying a change in the muscle protein secondary structure. Prerigor was least affected by brine-salting, having a final salt concentration of 2.2%, while postrigor had a NaCl content of 3.0% and frozen/thawed of 4.1%. Local variation within the fillets had an effect on the amide I absorption characteristics before as well as after salting. Salt uptake of the samples was affected by raw material quality and at the same time the degree of swelling of the myofibers was influenced by raw material character.

KEYWORDS: FT-IR microspectroscopy; Atlantic salmon; brine salting; prerigor; postrigor; frozen/thawed; microstructure; myofibrillar protein

INTRODUCTION

Salting has a long tradition as a preservation method for fish, and it is often used in combination with additional processing steps like smoking or drying. Both the salting process and the final product quality are highly influenced by the raw material characteristics, e.g., the rigor status of the fish or frozen storage. Rigor status and freezing/thawing before further processing will have an effect not only on fish flesh quality and the microstructure of fish muscle (*1, 2*) but also on the muscle proteins. The transition from prerigor to postrigor is closely related to changes in muscle biochemistry (*3*), one of the most obvious being changes in muscle pH (*4*). At the same time, these biochemical changes are accompanied by changes in the muscle microstructure (*5, 6*). In the prerigor state membranes are still intact, while enzymatic degradation of cellular structures will begin postrigor and with that the osmotic balance between intracellular and extracellular is gradually lost (*7*).

As different rigor stages affect the muscle architecture, frozen storage will likewise be accompanied by significant changes in microstructure and biochemical constitution (*8–11*). This is reflected by loss of water and changes in the texture of the fish flesh (*12, 13*). Frozen storage gives rise to mechanical damage through ice crystal formation (*9, 11*) and it may lead to changes in the muscle protein structure through dehydration (i.e., enhanced ion concentration in the muscle). Microstructural

* Corresponding author [phone +47-64-97-01-00; fax +47-64-97-03-33; e-mail ulrike.bocker@matforsk.no.

† Centre for Biospectroscopy and Data Modelling, Matforsk AS, Norwegian Food Research Institute.

‡ Department of Chemistry, Biotechnology and Food Science, Norwegian University of Life Sciences.

§ CIGENE, Centre for Integrative Genetics, Norwegian University of Life Sciences.

|| Department of Mathematical Sciences and Technology (IMT), Norwegian University of Life Sciences.

⊥ SINTEF Fisheries and Aquaculture AS.

Department of Biotechnology, Norwegian University of Science and Technology.

10.1021/jf703678z CCC: $40.75
Published on Web 06/10/2008

changes due to freezing, which occurred prior to processing, have an impact on final product quality as they can still be observed in smoked end products (*14*). The most sensitive of the myofibrillar proteins to freeze denaturation was found to be myosin (*15*).

Another process related factor influencing muscle texture and microstructure is the addition of NaCl. Increasing concentrations with a maximum around 5−6% are known to induce swelling of meat (*16–18*) and fish muscle, which is accompanied by an increase in water holding capacity. However, the uptake of salt and its distribution will be influenced by the raw material characteristics including rigor status, frozen storage, and share and distribution of fat in the fillet. The latter factor is known to have an inverted correlation to moisture content in the muscle (*19*). Diffusivity of salt is expected to decrease with increasing fat content as (*20*) found when comparing diffusivity values for several fish species with regard to varying fat levels. Similar effects related to fat content were lately reported by Gallart-Jornet et al. (2007) (*21*) when comparing salt diffusion in fatty and nonfatty fish species.

Salting itself will affect the stability of the myoproteins; in thermoanalytical studies with Differential Scanning Calorimetry (DSC) it was shown to decrease transition temperatures and peak areas (*22–25*). Changes observed in DSC are related to modifications in the thermal denaturation of proteins. It could be seen that salting decreased the heat stability of Actin and myosin (*25*). Fish myosin was found to be conformationally very unstable during handling and processing and the myosin heavy chain appeared to be the most vulnerable. Actin on the other hand was found more stable and its denaturation largely reversible apart from when severe heat denaturation conditions applied (*26*).

Vibrational spectroscopy has proven its potential for investigating process-induced changes in food muscle. Investigations by Raman spectroscopy on frozen stored hake indicated structural changes in the muscle proteins depending on the storage conditions (*27–29*). In addition it was reported that there might occur changes in protein−water interactions and muscle water structure (*30*). The major advantage of FT-IR microspectroscopy is that it offers the possibility to investigate protein secondary structural changes of tissue samples in situ with a similar sample preparation as required for conventional light microscopy. FT-IR microspectroscopy has been successfully applied for following the effects of salt- and/or heat-induced changes in the myofibrillar protein secondary structure of pork and beef (*31–34*). Spectral changes in the amide I region could be related to protein conformational changes, i.e., a decrease in α-helical structures and an increase in aggregated β-sheet structures during heating (*31, 32*). While with an increased salt concentration decreased share of α-helical components and higher share in non-hydrogenated C═O groups (1668 cm^{-1}) was related to increasing salt concentrations (*33*). A combined FTIR and Raman study on processed pork muscle tissue revealed further spectral areas—apart from the amide I region—that were affected by processing (*35*). In addition, process-induced changes in the protein secondary structure of pork muscle could be linked to changes in water mobility and distribution as observed by ^{1}H NMR relaxometry (*32, 34, 36*).

For salmon muscle, information about muscle protein structural changes and concomitant microstructural changes with respect to both raw material characteristics and brine salting is scarce. The aim of this study was to investigate the effects of brine salting on muscle microstructure and muscle protein secondary structure of Atlantic salmon with respect to fish raw quality. The experiment was carried out by brine-salting salmon fillets of three different raw material groups: prerigor, postrigor, and frozen/thawed. Sampling was performed on the head and the tail region of the fillet to account for local variation within the fillets. Microstructural appearance was investigated by light microscopy while protein secondary structural changes were analyzed by FT-IR microspectroscopy.

MATERIALS AND METHODS

Sample Preparation and Chemical Analysis. Nine farmed Atlantic salmon (*Salmo salar*) were commercially slaughtered and transported to the laboratory on ice. The average weight of all nine fish was 4.3 ± 0.8 kg. Three types of raw material were used for the experiment: prerigor (PrR), postrigor (PoR), and frozen/thawed (F/T) with three individuals in each group. One fillet per fish was used for collecting unsalted samples, while the other fillet was subjected to brine salting. The fish from group PrR were filleted and brine salted 3 h post mortem and the fish from group PoR after 72 h of storage on ice at 4 °C. Individuals from group F/T (frozen prerigor) were kept frozen at −20 °C for 3 weeks, before they were thawed, filleted, and brine salted. For all individuals the pH value was determined before and after the brine-salting procedure. The brine-salting process was carried out as follows: whole fillets were placed in brine containing 16% (w/v) NaCl at 4 °C with a ratio of 1:10 between fillets and brine. After 4 h they were removed from the brine and kept for another 14 h at 4 °C to allow further distribution of the salt in the fillets. Sampling for FT-IR microspectroscopy, light microscopy, and (wet) chemical analyses was done for each condition, i.e., before and after brine salting from the head and tail part for each individual from each group. The fat content was determined by using the method of Bligh and Dyer (*37*). Moisture content (*38*) was assessed by drying fillet homogenates (2 g) at 105 °C for 24 h. The salt content was determined according to the AOAC procedure (1990) (*39*) with the Vollhard method.

Light Microscopy. Muscle blocks 0.2 × 0.2 × 0.4 cm^3 in size were chemically fixed in 2.5% glutaraldehyde with 0.1 M cacodylate buffer (pH 7.3), and embedded in Technovit 7100 (Heraeus Kulzer, Wehrheim, Germany), which is a resin system based on glycol methacrylate. For all samples, 3 μm thick plastic sections were cut perpendicular to the myofibers, using a Leica RM2165 microtome (Leica Microsystems Wetzlar GmbH, Wetzlar, Germany). To carry out optical light microscopy the sections were stained with 1 g/100 mL Toluidine Blue (Sigma-Aldrich Norway AS, Oslo, Norway) to elucidate the general structure of the muscle samples. Due to the fact that in fish microstructural differences may occur locally, three blocks each from both the head and the tail of each animal were investigated. The sections were examined with a Leica DM 6000B microscope (Leica Microsystems Wetzlar GmbH, Wetzlar, Germany) and images were acquired at 100× magnification with an Evolution MP 5.0 CCD camera (MEDIA CYBERNETICS The Imaging Experts, Silver Springs, MD, USA). Two hundred fibers per sample were used to determine the fiber diameter, using Image-Pro Plus 4.5 (MEDIA CYBERNETICS The Imaging Experts, Silver Springs, MD, USA).

FT-IR Microspectroscopy. For FT-IR microspectroscopy, several muscle blocks of approximately 0.7 × 0.7 × 0.2 cm^3 were excised, embedded in OCT compound (Tissue-Trek, Electron Microscopy Sciences, Hatfiles, USA), and snap-frozen in liquid N_2. All samples were kept on dry ice before transfer to a −80 °C freezer where they were stored until cryo-sectioning.

Cryo-sectioning of the muscle blocks was performed transversely to the fiber direction on a Leica CM 3050 S cryostat (Leica Microsystems Wetzlar GmbH, Wetzlar, Germany). Ten micrometers thick sections were thaw-mounted on infrared transparent CaF_2 slides and stored overnight in a desiccator before collection of the FT-IR spectra.

FT-IR microspectroscopic data were collected via an IR Scope II connected to an Equinox 55 FT-IR spectrometer (Bruker Optik GmbH, Ettlingen, Germany) equipped with a liquid nitrogen-cooled mercury cadmium telluride (MCT) detector. IR spectra were acquired from single myofibers in transmission mode in the range from 4000 to 1000 cm^{-1}. The spectral resolution was at 6 cm^{-1} and measurements were made with a 15× objective lens. For each spectrum 256 interferograms were

Table 1. General Sample Characteristics of Unsalted Salmon Samples[a]

	samplename	weight [g]	moisture [%]	fat [%]	pH	fiberdiameter [μm]
prerigor	1(A)	4600	64.78 ± 0.24	17.66 ± 0.13	7.21	81.91 ± 28.16
	1(C)		72.54 ± 0.52	7.39 ± 0.94		77.98 ± 30.76
	2(A)	4500	68.01 ± 0.50	10.97 ± 0.35	7.11	91.37 ± 39.34
	2(C)		72.08 ± 0.34	5.95 ± 0.51		100.96 ± 30.12
	3(A)	3850	68.74 ± 0.54	10.35 ± 0.24	7.05	87.94 ± 25.85
	3(C)		71.53 ± 0.77	4.74 ± 0.03		84.37 ± 33.96
postrigor	4(A)	5500	68.63 ± 1.59	12.16 ± 0.26	6.19	84.39 ± 32.31
	4(C)		69.92 ± 0.57	9.24 ± 0.01		83.78 ± 31.18
	5(A)	3750	69.46 ± 0.21	10.45 ± 0.22	6.14	91.82 ± 29.42
	5(C)		71.87 ± 0.41	6.61 ± 0.35		93.52 ± 32.37
	6(A)	5600	69.68 ± 0.22	10.45 ± 0.01	6.21	87.02 ± 30.61
	6(C)		71.79 ± 0.41	6.68 ± 0.20		81.48 ± 31.67
frozen/thawed	7(A)	5550	69.66 ± 0.36	11.12 ± 0.09	6.35	90.46 ± 29.62
	7(C)		71.30 ± 3.02	5.64 ± 0.21		74.64 ± 30.40
	8(A)	4300	70.18 ± 0.14	8.59 ± 0.10	6.45	87.26 ± 27.12
	8(C)		71.26 ± 1.16	7.26 ± 0.44		86.26 ± 27.01
	9(A)	5850	66.19 ± 0.80	14.75 ± 0.31	6.33	87.36 ± 27.78
	9(C)		71.03 ± 0.57	10.43 ± 0.31		78.89 ± 27.30

[a] A indicates samples from the head and C samples from the tail part of the fillet.

coadded and averaged. The sealed microscope and the spectrometer were purged with dry air to reduce spectral contributions from water vapor and CO_2. A background spectrum of the CaF_2 substrate was recorded before each spectrum was measured to account for variations in water vapor and CO_2.

For every sample condition (i.e., quality, salt or no salt, head or tail) six spectra of single myofibers (three from two different locations on each cryo-section) were analyzed by microscpectroscpy. No spectra could be acquired for two sample conditions: unsalted PrR C fish #1 and salted PrR A fish #2. This resulted in a data set consisting of 204 (instead of 216 for a complete data set) spectra altogether. Of those 204 spectra 3 were detected as outliers and had to be removed leaving a data set accounting for 201 spectra.

Preprocessing and Multivariate Data Analysis of the FT-IR Spectra. Second derivatives were calculated to enhance the resolution of the spectral bands by applying a nine-point Savitzky−Golay filter (*40*). To separate physical light-scattering effects (as baseline, multiplicative, linear, and quadratic wavenumber dependent effects) from chemical information in spectra the infrared spectra were further preprocessed by using Extended Multiplicative Signal Correction (EMSC) (*41, 42*).

The data were analyzed by Principal Component Analysis (PCA) and Partial Least Squares Regression (PLSR) (*43*). PCA was used to explore differences in the spectral data between the three raw material groups.

To investigate the effect of the design on the spectral data and analysis of variance Partial Least Squares Regression (ANOVA-PLSR) (*43*) was applied with use of averaged spectra (one spectrum per experimental condition), using bands found in the second derivative spectra instead of using the whole spectral range to facilitate representation of the plots. For interpretation purposes the second derivative bands were multiplied by minus one for presentation purposes since minima in the second derivative correspond to the original spectral bands. In ANOVA-PLSR the design variables were used as the *X*-matrix and the FT-IR spectral data were used as the *Y*-matrix (*43*). The *X*-matrix for the design is defined by using 0 and 1 as indicator variables for the design factors. 0 or 1 indicated, if a certain condition applied for a sample or not. Here, each fish (numbered 1−9) was included in the design to account for potential individual differences within the three raw material groups. Chemical data were included in the *X*-matrix, however, in a pacified manner (weighted by 10^{-6}) to avoid their influence on the PLS model. The results of the ANOVA-PLSR were then studied by using so-called correlation loading plots. The correlation loading plot shows the correlation of the *X*- and *Y*-variables to the PLSR components which allows the investigation of how the design factors are correlated to the measured variables within the model. Validation was performed by full cross-validation.

Data analysis was carried out with Unscrambler version 9.2 (CAMO Process AS, Norway) and MATLAB version 7.3 (The MathWorks, Natick, MA).

RESULTS AND DISCUSSION

Chemical Characteristics and Microstructure. Table 1 gives an overview of the chemical characteristics of each individual sample in the unsalted state. In all three groups the fat content varied between about 5% and 15% depending on the sampling position on the fillet (head or tail). At the same time the moisture content in all groups ranged between approximately 66% and 73% showing an inverse relationship to fat content from head to tail position as is expected from previous reports (*19, 44*). The pH values for the prerigor group were all above pH 7, while pH was between 6.14 and 6.22 for the postrigor group and between 6.33 and 6.45 for the frozen/thawed group. **Table 2** summarizes the samples after brine salting. The pH dropped for prerigor to 6.57−6.63 due to the fact that the samples start to go in rigor during the salting process. The pH for the postrigor group stayed in the same range after salting (6.12−6.22), while for frozen/thawed samples it decreased about 0.3 units. The highest NaCl contents were found in the frozen/thawed fish, while the salt content increased least for prerigor fillets during brine salting. However, there are no obvious differences in salt uptake between the head and tail part in each sample group. This is rather unexpected since it was reported previously that salt uptake and diffusion depend on the fat content of a sample, but this was done by comparing the salt diffusion kinetics in a lean versus a fatty species (*21*). The fiber diameter change was about the same for postrigor and frozen/thawed samples with an average increase of about 10% in diameter. The average in diameter change for prerigor samples was 2%. However, it has to be kept in mind that fiber diameter can vary drastically over a small area in fish, which may explain the large individual differences (**Table 2**). The difference between the prerigor group and the other two groups may be explained by a lower salt uptake in the prerigor samples compared to postrigor and frozen/thawed. With a lower salt uptake the prerigor fish will thus experience less salt-induced swelling, as it is known that it is the salt ions that cause a weakening of oppositely charged protein side chains which contributes to the swelling process (*18*). The correlation loading plot in **Figure 1** showing PLS components 1 and 2 further illustrates the varying effect of brine salting on the different

Table 2. Sample Characteristics after 4 h of Brine Salting (16% NaCl) and a Subsequent Salt Distribution Time of 14 h[a]

	sample name	NaCl [%]	moisture [%]	NaCl/H_2O [%]	pH	fiberdiameter [μm]	change in fiber diameter [%]
prerigor	1(A)	1.38 ± 0.06	71.94 ± 1.40	1.92	6.63	94.60 ± 34.62	+15.49
	1(C)	1.32 ± 0.04	53.91 ± 9.34	2.45		76.06 ± 28.85	−2.46
	2(A)	1.57 ± 0.02	69.93 ± 6.34	2.25	6.57	92.80 ± 36.13	+1.57
	2(C)	1.47 ± 0.03	69.08 ± 0.45	2.13		78.06 ± 31.69	−22.68
	3(A)	1.90 ± 0.02	63.60 ± 0.69	2.99	6.57	98.29 ± 31.01	+11.77
	3(C)	1.13 ± 0.07	68.70 ± 0.41	1.65		82.45 ± 34.57	−2.28
postrigor	4(A)	1.47 ± 0.03	67.66 ± 0.41	2.17	6.12	99.66 ± 36.03	+18.09
	4(C)	2.59 ± 0.04	71.82 ± 0.10	3.61		92.27 ± 26.92	+10.09
	5(A)	2.19 ± 0.05	69.44 ± 0.24	3.16	6.22	109.22 ± 34.85	+18.95
	5(C)	2.04 ± 0.05	73.54 ± 0.77	2.78		78.96 ± 29.86	−15.57
	6(A)	1.87 ± 0.02	67.54 ± 0.18	2.77	6.14	95.93 ± 24.01	+10.24
	6(C)	2.37 ± 0.07	70.75 ± 0.24	3.35		98.54 ± 34.06	+20.94
frozen/thawed	7(A)	3.13 ± 0.01	66.97 ± 0.22	4.67	6.08	92.22 ± 28.55	+1.95
	7(C)	3.02 ± 0.32	71.31 ± 0.34	4.24		75.66 ± 28.80	+1.37
	8(A)	2.98 ± 0.05	68.72 ± 0.09	3.34	6.17	93.01 ± 29.77	+6.56
	8(C)	2.58 ± 0.04	71.32 ± 0.28	3.62		94.82 ± 31.91	+9.92
	9(A)	2.71 ± 0.04	66.47 ± 1.56	4.08	6.09	102.35 ± 30.14	+17.16
	9(C)	2.55 ± 0.01	70.60 ± 0.86	3.61		98.34 ± 38.34	+24.65

[a] A indicates samples from the head and C samples from the tail part of the fillet.

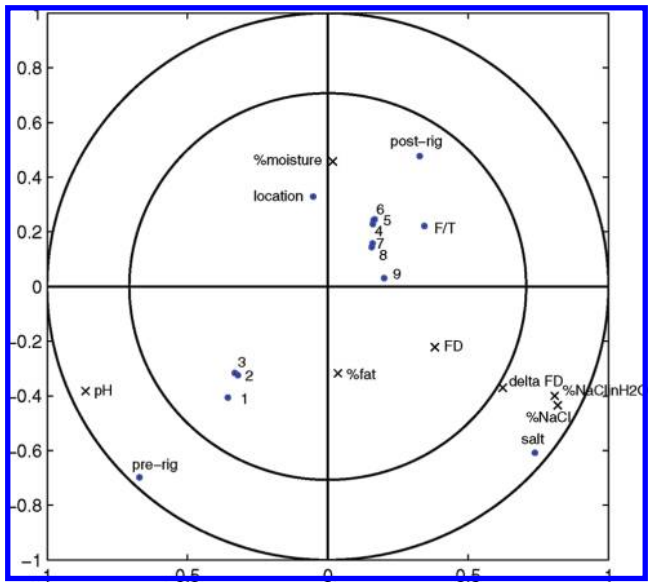

Figure 1. Correlation loading plot of ANOVA-PLSR with experimental design as *X* (marked by circles) and chemical characteristics of the samples as *Y* (marked by ×).

raw material groups: postrigor and frozen/thawed samples are related to higher salt contents and higher percent diameter increase opposed to samples from the prerigor group (PLS component 1). Furthermore, samples of the prerigor group clearly have the highest pH, while sample location is related to differences in fat and moisture content. To elucidate the accompanying microstructural changes **Figure 2** shows representative light micrographs of samples from the tail part of prerigor (a, d), postrigor (b, e), and frozen/thawed (c, f) salmon muscle unsalted (a−c) and salted in 16% brine (d−f). Before salting the three quality groups show striking differences in their microstructure. The prerigor muscle samples display a very dense architecture; the myofibers build a very tight lattice and it is hard to discriminate individual myofibers from each other. Samples from postrigor salmon show a less dense structure: individual muscle cells are more distinct, separated by a very noticeable endomysium. For frozen/thawed salmon muscle the extracellular matrix is considerably widened and the endomysium is partly disrupted. In addition, the myofibers appear shrunken and pale areas within the myofibers become visible. This agrees well with observations reported in the literature (*9, 14*). Bello et al. (1982) (*9*) pointed out that "holes" in the fibers are presumably caused by freeze-damage and are likely due to ice crystal formation in the sarcoplasm. The more open microstructure in the postrigor and frozen/thawed groups is fundamental for the increased salt uptake compared to prerigor samples (*20*).

After salting, the prerigor samples appear less dense than before salting. This may be due to the fact that these samples went into rigor during the brine-salting process. The rigor contraction of the prerigor samples will then oppose the salt-induced swelling of the myofibers. This might be an additional reason why these samples swell less compared to postrigor and frozen/thawed samples. Due to the salt-induced swelling in postrigor and frozen/thawed samples the extracellular space decreases again, which is most expressed for the frozen/thawed group.

FT-IR Microspectrosocpy. Figure 3 shows an average spectrum (average of 18 spectra from randomly selected myofibers) derived from spectra of unsalted postrigor salmon myofibers from the tail part of the fillet. This spectrum represents the most typical features seen for the three raw material groups investigated. It reveals very similar features to spectra acquired from beef or pork muscle myofibers (*31, 35*) and it is dominated by the amide I band between 1700 and 1600 cm^{-1}. To gain insight in changes related to the secondary structure of the myofibrillar proteins the amide I region (1700−1600 cm^{-1}) is investigated as second derivative spectra to enhance spectral resolution. The inset in **Figure 3** lays out two exemplary spectra which are averages of spectra collected from all three individuals of the PoR group and demonstrate overall typical features found in individual spectra. Nine bands could be determined in the amide I region. These bands were located at the following positions: 1694, 1682, 1668, 1659, 1653, 1639, 1628, 1619, and 1610 cm^{-1}, which were previously described for pork and beef muscle fibers (*31, 32*). The central band at 1653 cm^{-1} is diagnostic for α-helical structures which are present to over 90% in the rod part of the major myofibrillar myosin (*31, 32, 45*). The band at 1659 cm^{-1} is most likely related to loop structures and the band at 1668 cm^{-1} was previously related to nonhydrogenated C═O groups which involved only weak dipole−dipole interactions (*46*). The band components below 1640 cm^{-1} are commonly associated with intramolecular and the ones between 1610 and 1630 cm^{-1} aggregated (intermolecular) β-sheet structures (*46*). For the band at 1640 cm^{-1} it has to be kept in mind that there also is a strong nonprotein contribution

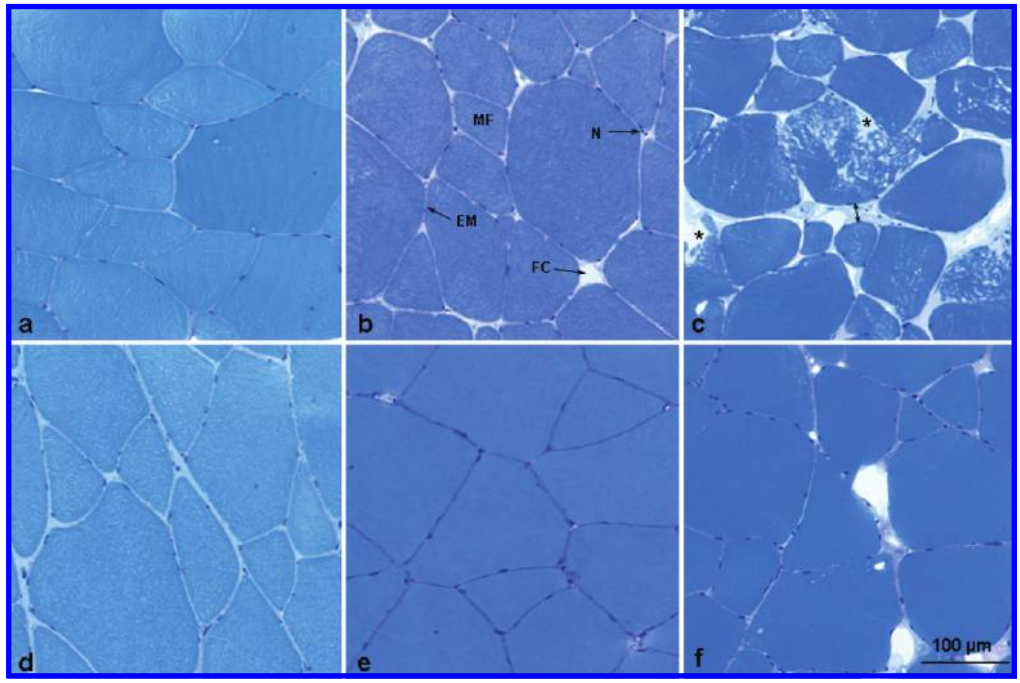

Figure 2. (**a**−**f**) Transverse sections of salmon muscle stained with Toluidine Blue. Images in the upper panel (a−c) show unsalted samples, the lower panel (**d**−**f**) show those from brine-salted samples. Panels a and d originate from prerigor, panels b and e from postrigor, and panels c and f from frozen/thawed salmon samples. All images shown were derived from the tail part of the salmon. Myofibers (MF), endomysium (EM), and nuclei (N) stain blue and (empty) fat cells (FC) appear unstained (widening of the extracellular matrix in frozen/thawed muscle is indicated by a the double-headed arrow; freezing artifacts are indicated by an asterisk).

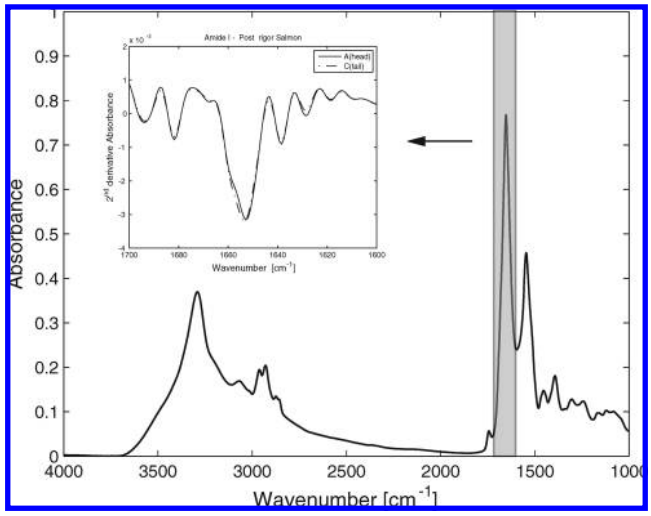

Figure 3. Typical FTIR spectrum of a single salmon muscle myofiber (postrigor tail part unsalted) showing the spectral range from 4000 to 1000 cm^{-1}. Inset: Second derivative average spectra of postrigor quality single muscle myofibers originating from the head and tail part of the salmon fillet.

from O−H bending of water at this position, which is overlapping with the low-frequency contribution of antiparallel β-sheets (*47*).

The overall features of second derivative spectra in the amide I region are similar for all three sample groups. However, it has to be acknowledged that there appears to be a major difference between spectra from the head (A) part and the tail (C) part. This is mainly reflected by an increased share of loop structures (1659 cm^{-1}) for the tail samples compared to the head samples. Similar differences between head and tail are found in the PrR and F/T groups, therefore head and tail are considered separately in the following.

Spectral Differences between Raw Materials. Principal component analysis (PCA) was used to investigate the variance of the myofiber spectra between the three groups of salmon in the amide I region between 1700 and 1600 cm^{-1}. **Figure 4a** shows the score plot of the first and second principal component based on 54 s derivative spectra in the amide I region from the head part and **Figure 4b** the score plot based on 48 spectra collected from unsalted salmon in the tail region of the fillet. The explained variances for PC 1 and PC 2 are 37% and 30% for the head part (**Figure 4a**) and are 57% and 21% for the tail part (**Figure 4b**). Higher principal components were studied; however, they did not reveal further information. The samples show an obvious clustering according to their raw material group (indicated by different colors) in both the head and tail part indicating differences in the amide I region of the spectra for the three fish qualities. Yet, some spectra of frozen/thawed of the head part which were all originating from the same individual (fish #9) were found near samples of the prerigor group (**Figure 4a**). In the tail part, the same individual (all six samples from fish #9 are located on the far right side) is explaining the main variation in PC 1. This indicates that individual variation has quite a strong influence in the spectral characteristics. However, it is unclear if the higher fat content in fish #9 compared to the two other individuals of the group alone is a sufficient explanation or if it is related to prerigor freeze/thaw effects on the proteins.

To illustrate the effect of the experimental design factors of unsalted samples on the spectral bands in the amide I region, ANOVA-PLSR was carried out and the correlation loading plot of the first two PLS components is shown in **Figure 5a**,b. Chemical characteristics of the samples were included in the *X*-matrix and were pacified to avoid their influencing the model. This procedure allows visualizing the chemical characteristics in the same correlation loading plot. For the head part samples (**Figure 5a**), the explained variances in *X* and *Y* for PLS

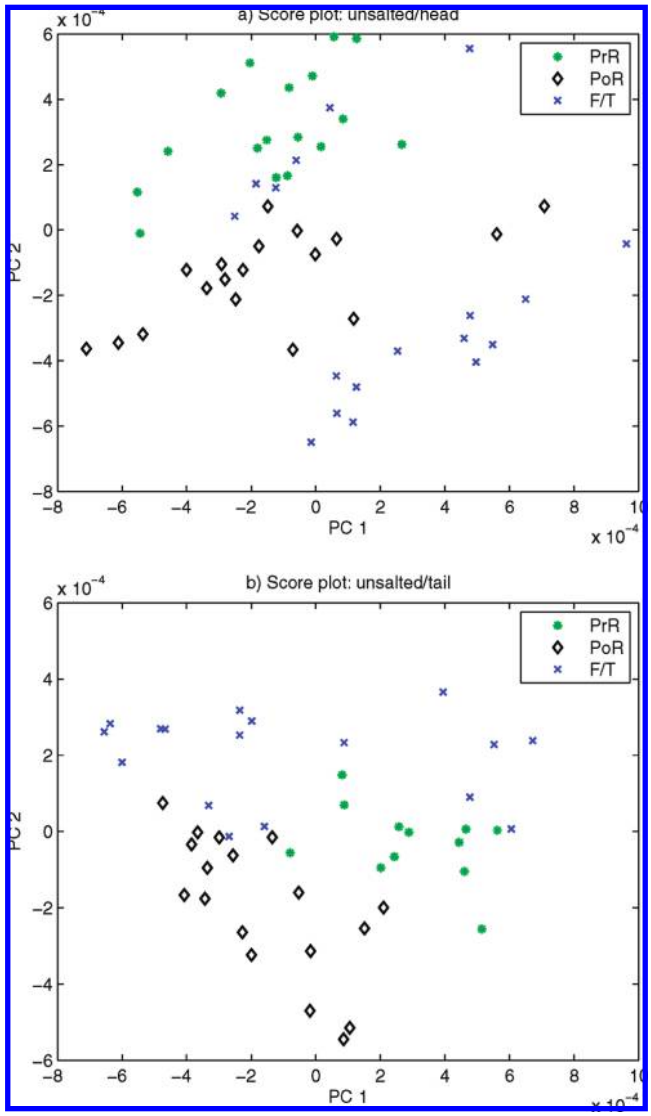

Figure 4. (a/b) PCA score plot of the variation between second derivative spectra in the range between 1700 and 1600 cm^{-1}: in green, prerigor; in black, postrigor; and in blue, frozen−thawed. (**a**) The explained variances for PC 1 and PC 2 are 37% and 30%, respectively. (**b**) The explained variances for PC 1 and PC 2 are 57% and 21%, respectively.

components 1 and 2 are 28% and 26% (for *X*) and 50% and 13% (for *Y*), respectively. The first PLS component is dominated by differences between prerigor (PrR) and frozen/thawed (F/T) samples. F/T samples appear highly related to both inter- and intramolecular β-sheet structures and nonhydrogenated C═O groups while they are opposed to PrR samples, i.e., PrR samples have less of these structures than the F/T samples. PoR samples are correlated with the α-helix band at 1653 cm^{-1} with a major contribution to PLS component 2. For the tail part samples (**Figure 5b**), the explained variances in *X* and *Y* for PLS components 1 and 2 are 31% and 22% (for *X*) and 34% and 39% (for *Y*), respectively. Here, the correlation loading plot reveals some different correlations than for the head part samples. PoR quality still appears to have most correlation to α-helical structures, while now PrR samples are related to nonhydrogenated C═O groups. However, F/T samples no longer show the same correlation to inter- and intramolecular β-sheet structures as in the head part samples. It is also possible that fish #9 is different from the rest of the group as already mentioned above. The reason for the differences between head and tail is unclear, but it has to be pointed out that the

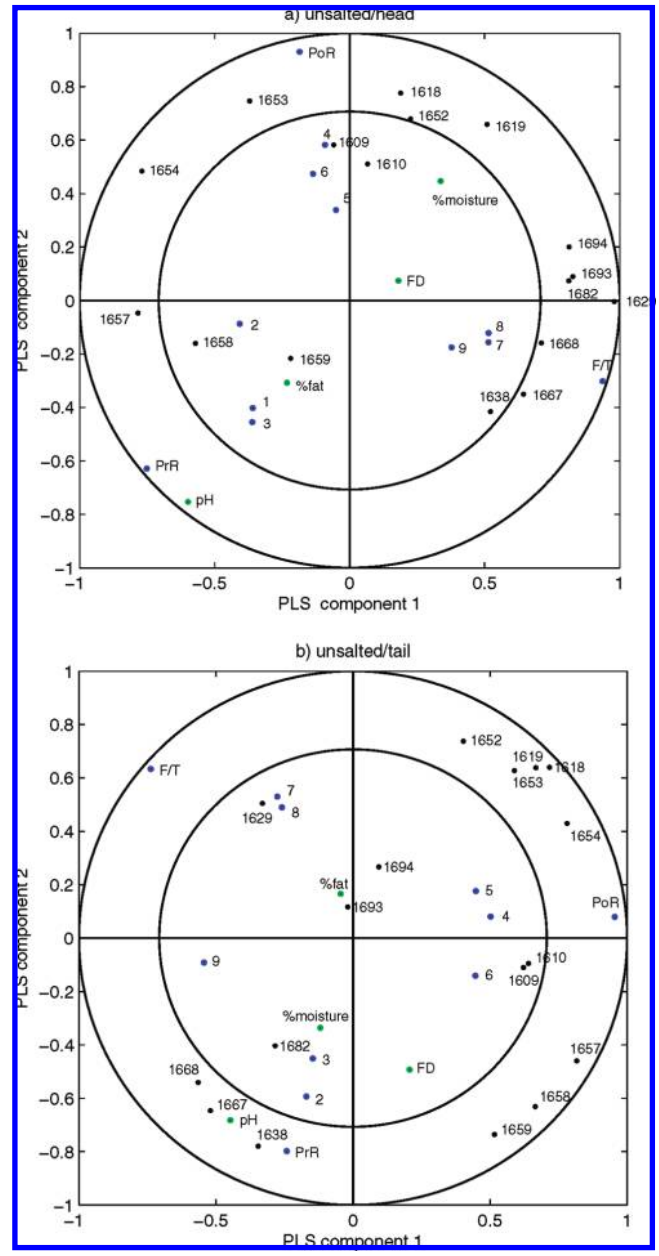

Figure 5. (a/b) Correlation loading plot of ANOVA-PLSR with design (in blue) and chemical characteristics of the samples as *X* (weighted by 10^{-6}; in green) and selected variables of the inverted second derivative of the amide I region of the FT-IR spectra as *Y* (in black). The inner and outer circle represent 50% and 100% explained variance. (**a**) The explained variances of PLS components 1 and 2 were 28% and 26% for *X* and 50% and 13% for *Y*, respectively. The optimal number of components was 1. (**b**) The explained variances of PLS components 1 and 2 were 31% and 22% for *X* and 34% and 39% for *Y*, respectively. The optimal number of components was 2.

environment of the myofibrillar proteins is possibly influenced by the different chemical characteristics in the head and tail part, i.e., the variation in moisture and fat content from head to tail. Furthermore, differences in thin filament proteins from head to tail were reported for largemouth bass white muscle (*48*). This observation has to be further investigated by focusing on a homogeneous raw material and possibly including the molecular composition with regard to head and tail.

Effect of Brine Salting on Spectral Characteristics with Regard to Raw Material. Again, principal component analysis was used to investigate the variance of the myofiber spectra

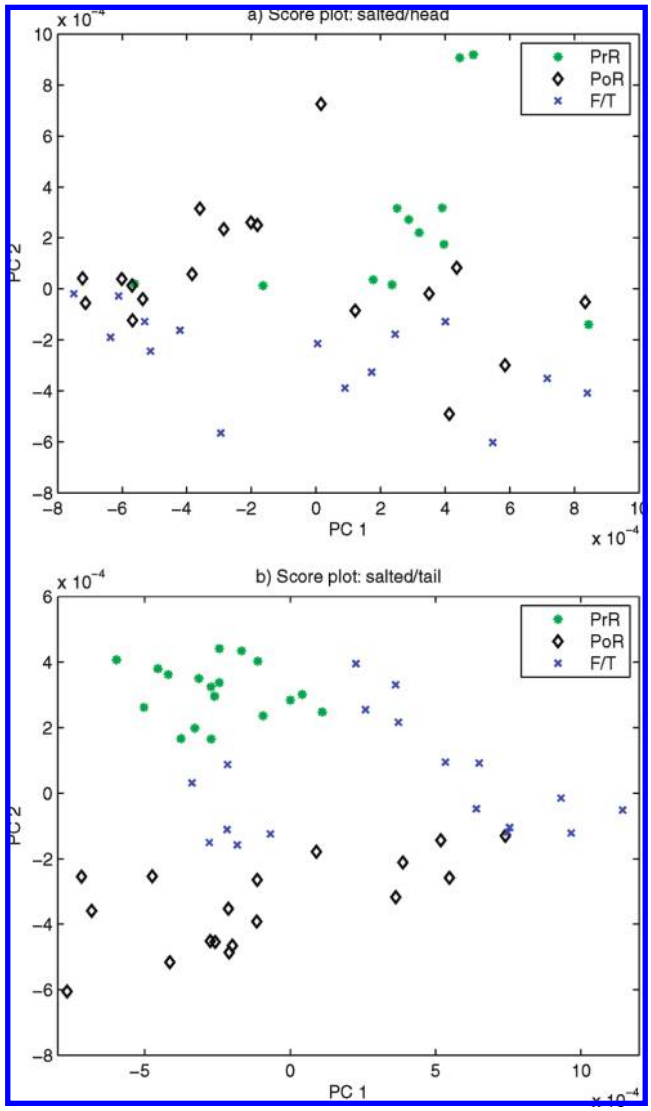

Figure 6. (a/b) PCA score plot of the variation between second derivative spectra in the range between 1700 and 1600 cm^{-1}: in green, prerigor; in black, postrigor; and in blue, frozen−thawed. (**a**) The explained variances for PC 1 and PC 2 are 49% and 22%, respectively. (**b**) The explained variances for PC 1 and PC 2 are 51% and 21%, respectively.

between the three groups of salmon in the amide I region between 1700 and 1600 cm^{-1}, this time for the salted samples. **Figure 6a** shows the score plot of the first and second principal component based on 45 s derivative spectra from the head part and **Figure 6b** the score plot based on 54 spectra collected from brine-salted salmon in the tail region of the fillet. The explained variances for PC 1 and PC 2 are 49% and 22% in for the head part (**Figure 6a**) and are 51% and 21% for the tail part (**Figure 6b**). Higher principal components, again, did not reveal further information. As in the unsalted state the samples show a clustering according to their raw material group (indicated by different colors) in both the head and tail part. However, in the head part individual #4 from the PoR group is found within the F/T group located toward the PrR group. In the tail region the clustering shows a much clearer separation between the three groups. As for the unsalted samples, ANOVA-PLSR with design parameters (including pacified chemical data) as *X*-matrix and amide I bands as *Y*-matrix was performed for both the head and tail samples separately. The respective correlation loading plots are shown in panels a and b of **Figure 7**. For the head part (**Figure 7a**), the first PLS component has an explained

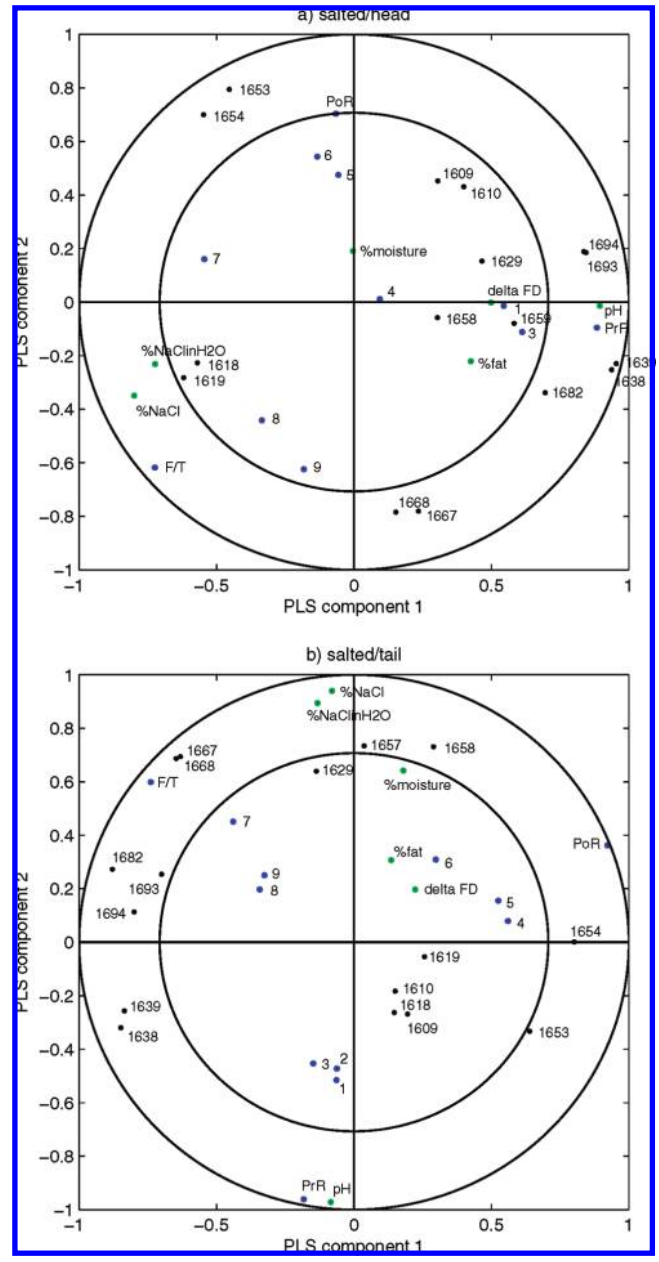

Figure 7. (a/b) Correlation loading plot of ANOVA-PLSR with design (in blue) and chemical characteristics of the samples as *X* (weighted by 10^{-6}; in green) and selected variables of the inverted second derivative of the amide I region of the FT-IR spectra as *Y* (in black). The inner and outer circle represent 50% and 100% explained variance. (**a**) The explained variances of PLS components 1 and 2 were 26% and 22% for *X* and 49% and 27% for *Y*, respectively. The optimal number of components was 1. (**b**) The explained variances of PLS components 1 and 2 were 28% and 27% for *X* and 42% and 25% for *Y*, respectively. The optimal number of components was 2.

variance of 26% and 49% for *X* and *Y*, respectively, while the second PLS component shows an explained variance of 22% and 27% in *X* and *Y*. After salting, the PrR group appears related to inter- and intramolecular β-sheet structures, while PoR appears related to α-helical structures. F/T samples, with the highest salt content, have some relation to nonhydrogenated C═O groups (PLS component 2) and the band at 1618/19 cm^{-1}. This corresponds to observations made in brine-salted pork muscle where a higher share in nonhydrogenated C═O groups (1668 cm^{-1}) was related to increasing salt concentrations (*33*). For the tail (**Figure 7b**), the first PLS component has an

explained variance of 28% and 42% for *X* and *Y*, respectively, while the second PLS component shows an explained variance of 27% and 25% in *X* and *Y*. The salted F/T group in the tail part shows a high correlation to the band at 1667/68 cm^{-1} (nonhydrogenated C═O). As before PoR samples are still associated with a higher share in α-helical structures. The PrR group, having the lowest salt content of all groups and highest pH, is inversely related to the band at 1657/58 cm^{-1} (loop structures), which seems to increase its share with increasing salt content. The PrR samples show different characteristics in the amide I region for head and tail after salting and a possible explanation is that not the lower salt uptake alone is responsible, but that in addition effects due to rigor effects and change in pH contribute to changes in the spectra. This has to be further investigated. Overall, individuals are much less spread within their groups in the tail region than in the head region. The wider distribution within groups in the head part accounts for all quality groups and not only for the frozen/thawed group as was seen for the unsalted samples.

The effect of brine salting on salmon muscle with regard to raw fish quality (prerigor, postrigor, frozen/thawed) was investigated by probing muscle microstructural changes by light microscopy and protein secondary structure by FT-IR microspectroscopy focusing on the amide I region. In general, the effect on the amide I region due to salting was smaller than that due to raw material and sampling location since the maximum NaCl concentration was only at about 4%. The salt uptake and final salt concentration varied due to the salmon raw material quality. After salt equilibration, F/T fish had a higher average salt content (4.1%) than PoR (3.0%), which in turn had a higher content than the PrR salmon (2.2%). This was ascribed to the more open structure of the F/T fish. Salted F/T, PoR, and PrR fish muscle revealed differences in the protein amide I region, i.e., in protein secondary structure. For F/T salmon, with 4.1% NaCl on average, the share of the 1668 cm^{-1} band increased referring to an increase of nonhydrogenated C═O groups. This is probably an effect of the higher salt concentration in this sample group compared to the other two. Before salting, there also existed spectral differences according to raw material; however, those were less systematic. PoR held the highest share of α-helical structure both before and after salting suggesting there was little effect on secondary structure due to salt, which was at 3%. Changes observed for PrR with regard to salting were very different for the head and tail part with an increase in β-structures in the head part while tail samples showed an inverse correlation to loop structures. The reason for this observation is unclear, since relatively small amounts of salt were taken up. However, the fish went through rigor during salting as their pH dropped. Swelling of the muscle fibers occurred to the same degree for F/T and PoR, but since changes in secondary structure did not appear to the same degree for both groups it can be concluded that swelling does not occur as a consequence of changes in protein secondary structure alone at these low salt concentrations. In addition, there were differences between the head and tail part for all three qualities. This was the case for fat and moisture content (more fat and less water in the head part) as well as for spectral characteristics in the amide I region which were mainly reflected by a higher share of loop structures in the tail region for all samples. These differences between the head and tail region did not, however, result in differences in salt uptake during brine salting.

FT-IR microspectroscopy proved to be a sensitive tool to observe process- and raw material-induced differences in fish muscle protein and offers a useful alternative for investigating related matters.

ACKNOWLEDGMENT

The authors would like to thank Vibeke Høst for her excellent technical assistance.

LITERATURE CITED

(1) Ando, M.; Toyohara, H.; Shimizu, Y.; Sakaguchi, M. Postmortem tenderization of Rainbow-Trout (Oncorhynchus-Mykiss) muscle caused by gradual disintegration of the extracellular-matrix structure. *J. Sci. Food Agric.* **1991**, *55*, 589–597.

(2) Nakayama, T.; Goto, E.; Ooi, A. Microstructure and physical properties of red sea-bream muscles stored as a fillet and as a round. *Fish. Sci.* **1997**, *63*, 950–957.

(3) Wang, D.; Tang, J.; Correia, L. R.; Gill, T. A. Postmortem changes of cultivated Atlantic salmon and their effects on salt uptake. *J. Food Sci.* **1998**, *63*, 634–637.

(4) Rustad, T. Muscle Biochemistry and the quality of wild and farmed cod. In *Quality assurance in the fish industry*; Huss, H. H., Jacobsen, M., Liston, J., Eds.; Elsevier: London, UK, 1992; pp 19−27.

(5) Ofstad, R.; Egelandsdal, B.; Kidman, S.; Myklebust, R.; Olsen, R. L.; Hermansson, A. M. Liquid loss as effected by post mortem ultrastructural changes in fish muscle: Cod (*Gadus morhua* L) and salmon (*Salmo salar*). *J. Sc. Food Agric.* **1996**, *71*, 301–312.

(6) Olsson, G. B.; Olsen, R. L.; Ofstad, R. Post-mortem structural characteristics and water-holding capacity in Atlantic halibut muscle. *Lebensm.-Wiss.-Technol.* **2003**, *36*, 125–133.

(7) Rora, A. M. B.; Furuhaug, R.; Fjaera, S. O.; Skjervold, P. O. Salt diffusion in pre-rigor filleted Atlantic salmon. *Aquaculture* **2004**, *232*, 255–263.

(8) Bello, R. A.; Luft, J. H.; Pigott, G. M. Improved histological procedure for microscopic demonstration of related changes in fish muscle-tissue structure during holding and freezing. *J. Food Sci.* **1981**, *46*, 733.

(9) Bello, R. A.; Luft, J. H.; Pigott, G. M. Ultrastructural-study of skeletal fish muscle after freezing at different rates. *J. Food Sci.* **1982**, *47*, 1389–1394.

(10) Foucat, L.; Taylor, R. G.; Labas, R.; Renou, J. P. Characterization of frozen fish by NMR imaging and histology. *Am. Lab.* **2001**, *33*, 38–43.

(11) Ayala, M. D.; Albors, O. L.; Blanco, A.; Alcazar, A. G.; Abellan, E.; Zarzosa, G. R.; Gil, F. Structural and ultrastructural changes on muscle tissue of sea bass, *Dicentrarchus labrax* L., after cooking and freezing. *Aquaculture* **2005**, *250*, 215–231.

(12) Mackie, I. M. The effects of freezing on flesh proteins. *Food Rev. Int.* **1993**, *9*, 575–610.

(13) Morkore, T.; Hansen, A. A.; Unander, E.; Einen, O. Composition, liquid leakage, and mechanical properties of farmed rainbow trout: Variation between fillet sections and the impact of ice and frozen storage. *J. Food Sci.* **2002**, *67*, 1933–1938.

(14) Sigurgisladottir, S.; Ingvarsdottir, H.; Torrissen, O.; Cardinal, M.; Hafsteinsson, H. Effects of freezing/thawing on the microstructure and the texture of smoked Atlantic salmon (*Salmo salar*). *Food Res. Int.* **2000**, *33*, 857–865.

(15) Careche, M.; del Mazo, M. L.; Fernandez-Martin, F. Extractability and thermal stability of frozen hake (*Merluccius merluccius*) fillets stored at−10 and−30 °C. *J. Sci. Food Agric.* **2002**, *82*, 1791–1799.

(16) Offer, G.; Trinick, J. On the mechanism of water holding in meat: the swelling and shrinking of myofibrils. *Meat Sci.* **1983**, *8*, 245–281.

(17) Offer, G.; Knight, P. The structural basis of water-holding in meat Part 1: General principles and water uptake in meat processing. In *Developments in Meat Science*; Lawrie, R., Ed.; Elsevier Science Publishers Ldt: Barking, Essex, UK, 1988; Vol. 4, pp 63−172.

(18) Honikel, K. O. The meat aspects of water and food quality. In *Water and Food Quality*; Hardman, T. M., Ed.; Elsevier Applied Science: London and New York, 1989.
(19) Aursand, M.; Bleivik, B.; Rainuzzo, J. R.; Jorgensen, L.; Mohr, V. Lipid Distribution and Composition of Commercially Farmed Atlantic Salmon (*Salmo salar*). *J. Sci. Food Agric.* **1994**, *64*, 239–248.
(20) Wang, D. H.; Tang, J. M.; Correia, L. R. Salt diffusivities and salt diffusion in farmed Atlantic salmon muscle as influenced by rigor mortis. *J. Food Eng.* **2000**, *43*, 115–123.
(21) Gallart-Jornet, L.; Barat, J. M.; Rustad, T.; Erikson, U.; Escriche, I.; Fito, P. A comparative study of brine salting of Atlantic cod (*Gadus morhua*) and Atlantic salmon (*Salmo salar*). *J. Food Eng.* **2007**, *79*, 261–270.
(22) Kijowski, J. M.; Mast, M. G. Effect of sodium-chloride and phosphates on the thermal properties of chicken meat proteins. *J. Food Sci.* **1988**, *53*, 367.
(23) Park, J. W.; Lanier, T. C. Scanning calorimetric behavior of Tilapia myosin and Actin due to processing of muscle and protein-purification. *J. Food Sci.* **1989**, *54*, 49–51.
(24) Schubring, R. Differential scanning calorimetric investigations on pyloric caeca during ripening of salted herring products. *J. Thermal Anal. Calorim.* **1999**, *57*, 283–291.
(25) Thorarinsdottir, K. A.; Arason, S.; Geirsdottir, M.; Bogason, S. G.; Kristbergsson, K. Changes in myofibrillar proteins during processing of salted cod (*Gadus morhua*) as determined by electrophoresis and differential scanning calorimetry. *Food Chem.* **2002**, *77*, 377–385.
(26) Hastings, R. J.; Rodger, G. W.; Park, R.; Matthews, A. D.; Anderson, E. M. Differential scanning calorimetry of fish muscle—the effect of processing and species variation. *J. Food Sci.* **1985**, *50*, 503.
(27) Careche, M.; LiChan, E. C. Y. Structural changes in *cod myosin* after modification with formaldehyde or frozen storage. *J. Food Sci.* **1997**, *62*, 717–723.
(28) Careche, M.; Herrero, A. M.; Rodriguez-Casado, A.; Del Mazo, M. L.; Carmona, P. Structural changes of Hake (*Merluccius merluccius* L.) fillets: Effects of freezing and frozen storage. *J. Agric. Food Chem.* **1999**, *47*, 952–959.
(29) Herrero, A. M.; Carmona, P.; Careche, M. Raman spectroscopic study of structural changes in hake (*Merluccius merluccius* L.) muscle proteins during frozen storage. *J. Agric. Food Chem.* **2004**, *52*, 2147–2153.
(30) Herrero, A. A.; Carmona, P.; Garcia, M. L.; Solas, M. T.; Careche, M. Ultrastructural changes and structure and mobility of myowater in frozen-stored hake (*Merluccius merluccius* L.) muscle: Relationship with functionality and texture. *J. Agric. Food Chem.* **2005**, *53*, 2558–2566.
(31) Kirschner, C.; Ofstad, R.; Skarpeid, H.-J.; Høst, V.; Kohler, A. Monitoring of denaturation processes in aged beef loin by Fourier transform infrared microspectroscopy. *J. Agric. Food Chem.* **2004**, *52*, 3920–3929.
(32) Bertram, H. C.; Kohler, A.; Böcker, U.; Ofstad, R.; Andersen, H. J. Heat-induced changes in myofibrillar protein structures and myowater of two pork qualities. A combined FT-IR spectroscopy and low-field NMR relaxometry study. *J. Agric. Food Chem.* **2006**, *54*, 1740–1746.
(33) Böcker, U.; Ofstad, R.; Bertram, H. C.; Egelandsdal, B.; Kohler, A. Salt-induced changes in pork myofibrillar tissue investigated by FT-IR microspectroscopy and light microscopy. *J. Agric. Food Chem.* **2006**, *54*, 6733–6740.
(34) Wu, Z. Y.; Bertram, H. C.; Kohler, A.; Bocker, U.; Ofstad, R.; Andersen, H. J. Influence of aging and salting on protein secondary structures and water distribution in uncooked and cooked pork. A combined FT-IR microspectroscopy and H-1 NMR relaxometry study. *J. Agric. Food Chem.* **2006**, *54*, 8589–8597.
(35) Böcker, U.; Ofstad, R.; Wu, Z.; Bertram, H. C.; Sockalingum, G. D.; Manfait, M.; Egelandsdal, B.; Kohler, A. Revealing co-variance structures in FT-IR and Raman microspectroscopy spectra—A study on pork muscle fiber tissue subjected to different processing parameters. *Appl. Spectrosc.* **2007**, *61*, 1032–1039.
(36) Wu, Z.; Bertram, H. C.; Böcker, U.; Ofstad, R.; Kohler, A. Myowater dynamics and protein secondary structural changes as affected by heating rate in three pork qualities: A combined FT-IR microspectroscopic and ^{1}H NMR relaxometry study. *J. Agric. Food Chem.* **2007**, *55*, 3990–3997.
(37) Bligh, E. G.; Dyer, W. J. A Rapid Method of Total Lipid Extraction and Purification. *Can. J. Biochem. Physiol.* **1959**, *37*, 911–917.
(38) Nordisk Metodikkommite for næringsmidler, NMKL-metode no. 23. 1991.
(39) *Official Method of Analysis of AOAC International*, 15th ed.; AOAC: Arlington, VA, 1990; Vol. 2, p 870.
(40) DeNoyer, L. K.; Dodd, J. G. Smoothing and derivatives in spectroscopy. In *Handbook of Vibrational Spectroscopy*; Chalmers, J. M., Griffiths, P. R., Eds.; John Wiley & Sons Ltd.: Chichester, UK, 2002; Vol. 3, pp 2173−2183.
(41) Martens, H.; Stark, E. Extended multiplicative signal correction and spectral interference subtraction—New preprocessing methods for near-infrared spectroscopy. *J. Pharm. Biomed. Anal.* **1991**, *9*, 625–635.
(42) Kohler, A.; Kirschner, C.; Oust, A.; Martens, H. Extended multiplicative signal correction as a tool for separation and characterisation of physical and chemical information in Fourier transform infrared microscopy images of cryo-sections of beef loin. *Appl. Spectrosc.* **2005**, *59*, 707–716.
(43) Martens, H.; Martens, M. *Multivariate Analysis of Quality: An Introduction*; John Wiley & Sons Ltd: Chichester, UK, 2001.
(44) Bell, J. G.; McEvoy, J.; Webster, J. L.; McGhee, F.; Millar, R. M.; Sargent, J. R. Flesh lipid and carotenoid composition of Scottish farmed Atlantic salmon (*Salmo salar*). *J. Agric. Food Chem.* **1998**, *46*, 119–127.
(45) Nakaya, M.; Watabe, S.; Ooi, T. Differences in the thermal-stability of acclimation temperature-associated types of Carp myosin and its rod on differential scanning calorimetry. *Biochemistry* **1995**, *34*, 3114–3120.
(46) Jackson, M.; Mantsch, H. H. The use and misuse of FTIR spectroscopy in the determination of protein-structure. *Crit. Rev. Biochem. Mol. Biol.* **1995**, *30*, 95–120.
(47) Jackson, M.; Choo, L. P.; Watson, P. H.; Halliday, W. C.; Mantsch, H. H. Beware of connective-tissue proteins—assignment and implications of collagen absorptions in infrared-spectra of human tissues. *Biochim. Biophys. Acta* **1995**, *1270*, 1–6.
(48) Thys, T. M.; Blank, J. M.; Coughlin, D. J.; Schachat, F. Longitudinal variation in muscle protein expression and contraction kinetics of largemouth bass axial muscle. *J. Exp. Biol.* **2001**, *204*, 4249–4257.

Received for review December 17, 2007. Revised manuscript received March 21, 2008. Accepted April 2, 2008. This work was supported through grant 153381/140 financed by the Research Council of Norway.

JF703678Z